Asian Journal of Chemistry; Vol. 32, No. 12 (2020), 3113-3119

ASIAN JOURNAL OF CHEMISTRY

https://doi.org/10.14233/ajchem.2020.22936

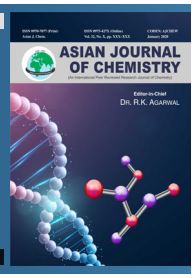

# Fabrication and Characterization of Chitosan-Polypyrrole/Strontium-Magnesium Substituted Hydroxyapatite Biocomposite with Potential Application in Tissue Engineering Scaffolds

P. LAVANYA[1,2,*], N. VIJAYAKUMARI[1,*], R. SANGEETHA[1,3] and G. PRIYA[1,3]

[1]Department of Chemistry, Government Arts College for Women, Salem-636008, India
[2]Department of Chemistry, Vivekanandha College for Arts and Science for Women, Veerachipalayam, Sankari-637303, India
[3]Department of Chemistry, Shri Sakthikailassh Women's College, Salem-636003, India

*Corresponding author: E-mail: srilavs870@gmail.com

*Received*: 8 August 2020; *Accepted*: 1 October 2020; *Published online*: 7 December 2020; AJC-20149

Biocomposite scaffolds of strontium-magnesium substituted hydroxyapatite (SMHA) with a mixture of chitosan/polypyrrole (CS-PPY) have been prepared by solvent casting method. The synthesized SMHA nanoparticles and biocomposite scaffold were characterized by FTIR, XRD and SEM techniques. The SEM morphology revealed the porous structure of the scaffolds designed for the muticomponents. The biomineralization and cell viability of the biocomposite were assessed *via* alkaline phosphatase activity and MTT assay on the osteoblast cell line. The study demonstrated improved differentiation and mineralization of osteoblast cells in the designed biocomposite scaffolds. The dye stained fluorescent microscopic photographs apparent the good scattering and permeability of cells onto the scaffolds. However, biocomposite demonstrated good antibacterial activity and the excellent biocompatibility against osteoblast cells offers a possible route for the production of a biocomposite as a viable replacement for regenerative medicine scaffolding substance.

**Keywords: Bone, Biocomposite, Hydroxyapatite, Scaffolds, Tissue engineering.**

## INTRODUCTION

The extracellular matrix (ECM) of the bone is extremely complex and consisting of both organic and inorganic constituents [1]. The organic component is made up of lipids, non-collagen and collagen protein. The principal inorganic portion of the ECM of bone is hydroxyapatite [2]. Hence, the biomaterial bone defect filling consisting of both inorganic and organic substances imitating the ECM of the bone may have a greater regenerative capacity of the bone tissue. Due to its specific characteristics such as surface-to-volume, tunability physical features in terms of surface chemistry, thickness and form, hydroxyapatite has generated interest in the field of biomedical applications [3]. Hydroxyapatite is biomimetic, osteoinduction, bioresorbable and has an almost identical biochemical and crystalline structure to the natural bone apatite. Nanostructures biomaterial alteration may have a beneficial impact on cell activity and the division of stem cells. Many of the biomaterials focused on nano-hydroxyapatite, therefore, ignore osteoinductivity. The mineralized layer of enamel, bone includes hydroxyapatite, partly enhanced instead of calcium by a broad range of substituted ions. Within nano-hydroxyapatite crystals, calcium can be substituted/reconstructed with magnesium, strontium, fluoride or phosphate affecting the biological function of the components [4]. Strontium promotes bone production and prevents the resorption of osteoclast skeletons. Strontium substituted hydroxyapatite biocomposites filled with bone marrow derived mesenchymal stem cells (BMSCs) have achieved superior osteogenic abilities and may facilitate osteoporotic tissue repair [5]. Magnesium plays a significant part in the cycle of calcification, tends to minimize bone fragile nature and has an observable impact on bone metabolism. This has also been stated to have a major contributor to the reduction of potential osteoarthritis chronic diseases in humans [6]. Both strontium and magnesium may also be integrated into nano hydroxyapatite to enhance hydroxyapatite crystalline structure and osteoinductivity.

Organic ingredients such as collagen, silk fibroin chitosan, polyethyleneterephthalate, polytetrafluoroethylene and polypyrene are also used to enhance the cytocompatibility and osteo-

induction of bone regeneration biomaterials. Polypyrrole (PPY) is among specific conducting polymers a very promising leading polymer, with remarkable characteristics such as simple synthesis, environmental resilience, outstanding electrical, optical, electro-chemical and mechanical properties, which have led to multiple applications in the various industries and biomedical industries. In addition to these remarkable characteristics, low processability prevents safe polypyrrole for a wide spectrum of medical applications [7]. In this specific context, one way of fulfilling the necessity and compensating for the deficiencies is to blend nanoparticle polypyrrole with other composites from internal or external sources to synthesize a polymer biocomposite that incorporates the good attributes of both materials. The matrix must be cytocompatible, degradable, non-hazardous, and meet certain clinical criteria for the usage of such biocomposites in medicinal use.

Chitosan is a perfect choice that satisfies all the criteria can be called an outstanding matrix [8]. Chitosan was especially noted for its outstanding characteristics such as excellent film-forming capacities, degradability, biocompatibility, low cytotoxicity, wettability, biofunction, antimicrobial activity and outstanding protein compatibility [9]. As per the excellent characteristics described above, including specific future, chitosan (CS) and polypyrrole (PPY) use, corresponding research centered on the usage of CS-PPY in medical applications taking into consideration the possible uses of CS-PPY biocomposites, thorough comprehension of bio, physical-chemical and dielectric relaxation properties is the major challenge.

The goal of this study was to explore biocomposites with the introduction of nano-hydroxyapatite dependent on mixtures of polymers. The fact of hydroxyapatite is useful for enhancing material characteristics while reducing the substance′s porosity. With our full understanding, the use of ternary chitosan, polypyrrole blend for the preparation of a hydroxyapatite biocomposite has not yet been reported.

## EXPERIMENTAL

**Synthesis of strontium-magnesium substituted hydroxyapatite (SMHA) nanoparticles:** For preparing Sr-Mg substituted hydroxyapatite nanoparticles, a standard sol-gel assisted synthesis technique was implemented [10]. Different amounts were mixed in deionized water to form solution A for the source minerals calcium strontium and magnesium ions (0.5 M). In next stage, 0.3 M $(NH_4)_2HPO_4$ and 0.3 M EDTA were dissolved to form solution B using deionized water. For all the solutions, the calcium substituent: phosphate molar ratio was set to 1.67. Consequently, solution B was introduced at room temperature dropwise into solution A with continuous stirring for 2 h. A NaOH solution was used to keep the pH around 10. The collected suspension was stored for 24 h at 50 ºC, the precipitate was drained off and rinsed with deionized water and ethanol several times. The resulting gel was dried in an oven at 100 ºC for 24 h and then calcined in a muffle furnace at 500 ºC for 4 h at a heating rate of 20 ºC/min.

**Preparation of CS-PPY/SMHA biocomposite:** The CS-PPY/SMHA biocomposite was used with casting/solvent removal processing [11]. Initially, chitosan (2 g) was dissolved at ambient temperature by vortex stirring in 1% acetic acid solution (100 mL). Added of 20 % of SMHA nanoparticles to the above CS-PPY solution with the constant sonication to acquire the uniform CS-PPY/SMHA suspension. The CS-PPY/SMHA biocomposite solution was consequently cast on the glass plate and allows the drying of CS-PPY/SMHA films at 37 ºC for 2 days.

**Characterization:** X-ray diffraction spectrometry was obtained using Cu*K*α radiation with XRD (DX-2000). The FTIR spectra are measured with a NICOLET 200SXV Infrared spectrophotometer at room temperature. The SEM and TEM analyses were performed using JSM-5900LV, JEOL and H-6009IV, Hitachi, instruments, respectively. The biocomposite material characteristics have been assessed using a testing machine (AI-7000-M, Gotech Testing Machine Inc.).

**Swelling studies:** For the swelling study, the biocomposite was kept in deionized water at room temperature. At that point, tests were taken out and gauged after delicate surface cleaning with permeable paper at a normal time frame until balance growing was reached. The equilibrium swelling ratio (SR) is characterized as the proportion of swollen load to the underlying weight [12].

**Biodegradation:** The biodegradation of the biocomposite platforms was concentrated in PBS enclosing lysozyme at room temperature. Biocomposite was submerged in PBS and hatched at room temperature for 7, 14 and 21 days. Introductory loads of the biocomposite was gotten as $W_o$ and after inundation, the biocomposite were washed in refined water to evacuate the surface adsorbed particles and casting [13].

**Antimicrobial activity:** The antimicrobial movement was assessed by the development hindrance examine utilizing the technique described elsewhere [14].

**Alkaline phosphatase activity (ALP):** Osteogenic separation of the bone cells was surveyed by ALP. The ALP assay procedure was adopted from an earlier report [15].

**Measurement of cytotoxicity:** The biocompatibility of the biocomposite was evaluated by deciding the suitability of the MG-63 osteoblast cells because of the molded media utilizing MTT measures. Quickly, biocomposite plates were cleaned in 70% ethanol followed by washing in a sterile PBS. Osteoblast cells were seeded on the biocomposite surface in a 96-well plate with DMEM enhanced with 10% FBS and swelled at room temperature for 3 days in 5% $CO_2$. Subsequently, the solution was supplanted with MTT and kept for another 5 h. At last, 100 µL of DMSO was included with delicate blending in a shaker. The cell culture medium with no treatment was considered as control [16].

**Statistics:** Every quantitative results was acquired from triplicate and reported as a mean ± standard deviation.

## RESULTS AND DISCUSSION

**FTIR studies:** Hydroxyapatite-associated functional group bands were detected with FTIR spectroscopy. Fig. 1a displays the FTIR spectrum for the pre-produced SMHA nanoparticles. The vibration of ion stretching at 3515 $cm^{-1}$ indicates the existence of an $OH^-$ group. As recorded earlier [17], other extending vibrations have also been observed for $CO_3^{2-}$ and $PO_4^{3-}$ func-

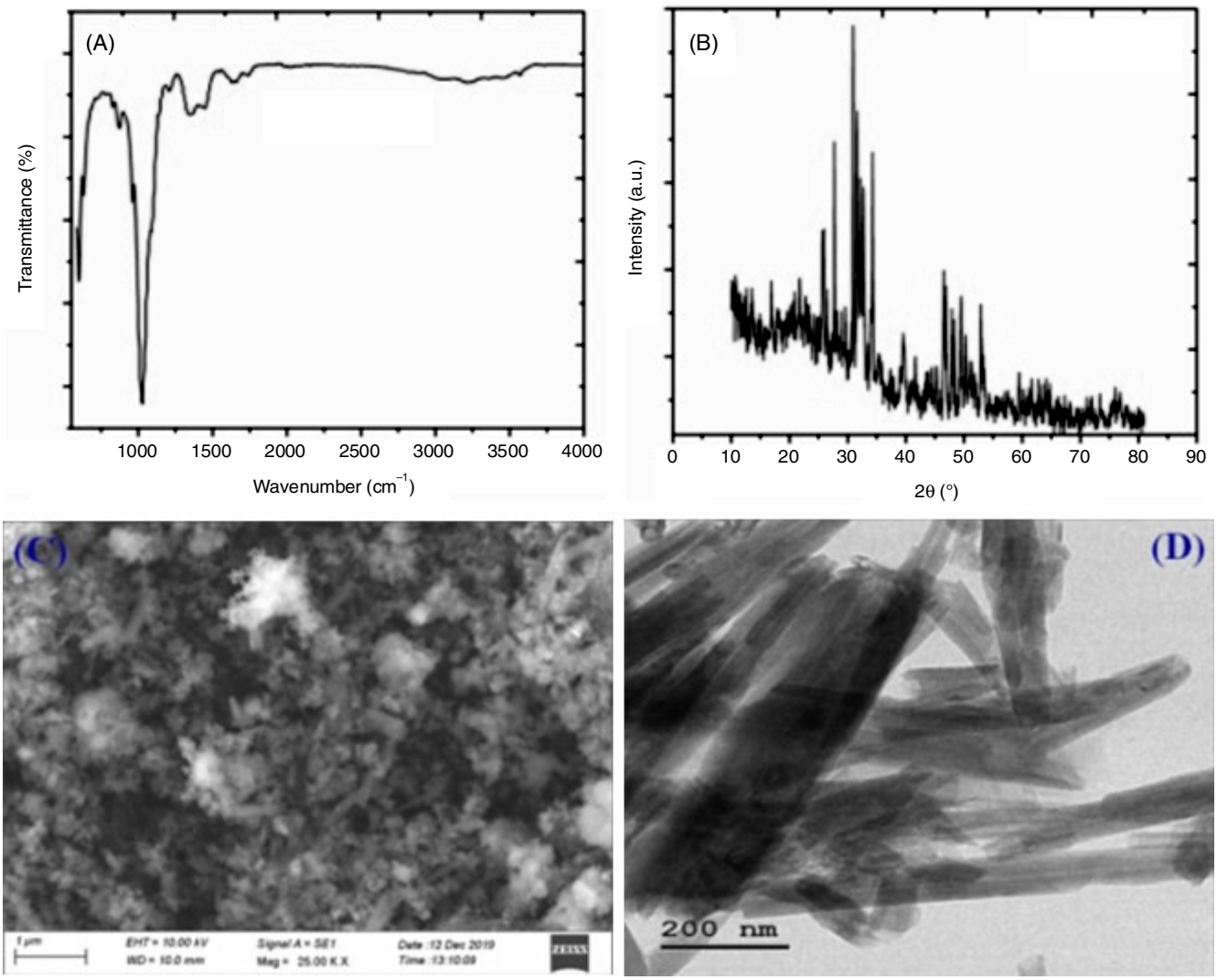


Fig. 1. (a) FTIR spectra (b) X-ray diffraction spectra (c & d) SEM and TEM of prepared SMHA nanoparticles

tional groups. Phosphate functional group consists of 600-560 and 1100-1000 cm$^{-1}$ intense FTIR absorption peaks. A fairly large $H_2O$ band with an apparent band from 3600 to 2600 cm$^{-1}$ forms a weaker band at 640 cm$^{-1}$. Intensive bands of $CO_3^{2-}$ between 1468 and 1550 cm$^{-1}$ reflecting neat hydroxyapatite [18].

**XRD studies:** The X-ray diffraction patterns of SMHA nanoparticles display the sharper peaks which suggest a greater crystallinity (Fig. 1b). The peak positions correspond well to the JCPDS card No. 896438 [19]. A well-resolved, high-intensity peak was reached for SMHA at 2θ of 31° equal to 211 planes. In the prepared SMHA powders, a typical accompanying plane in pure hydroxyapatite (*viz.* 321, 132, 222, 203, 131, 202, 211, 002, 200) is well identified. The X-ray diffraction patterns out-comes of the present study are consistent with the previous results [20].

**Morphological studies:** Fig. 1c displays the morphologies of prepared SMHA biocomposites. All the SMHA samples consist of fine-grained particulate matter and uniform component distribution. Scanning electron microscopic pictures display the morphological nanorod formations similar to the structure of human bone [21]. SMHA nanorods were ranged between 50 and 165 nm in width; and length between 230 and 650 nm. Fig. 1d shows the TEM images of SMHA nanoparticles, which demonstrates the morphology in the form of a rod or needle. The comparative study assumes that the samples are in line with standard form and structure.

**Characterization of biocomposite:** Due to O-H and N-H interaction of stretching vibrations (Fig. 2a), IR of the biocomposite displayed the wide absorption peaks centered between 3450 and 3100 cm$^{-1}$ [22]. The peaks were significantly wider than the peaks found in the chitosan and polypyrrole (PPY) owing to prolonged hydrogen fluctuations (O–HN, O–HO, N –HO) [22]. As seen in the composite FT-IR spectrum, the wide peaks appeared at 1660-1600 cm$^{-1}$ due to the mixture of chitosan and polypyrrole peaks observed at the same length.

With the introduction of SMHA nanoparticles in the biocomposite, a minor shift was found in the CS-PPY composite in the N-H bending section, attributable to the contact between the composite and SMHA nanoparticles [23]. In addition, a characteristic band of 921 cm$^{-1}$ was also observed, which conformed the P-O bending in the SMHA nanoparticles. The CS-PPY matrix had been packed with SMHA nanoparticles. The

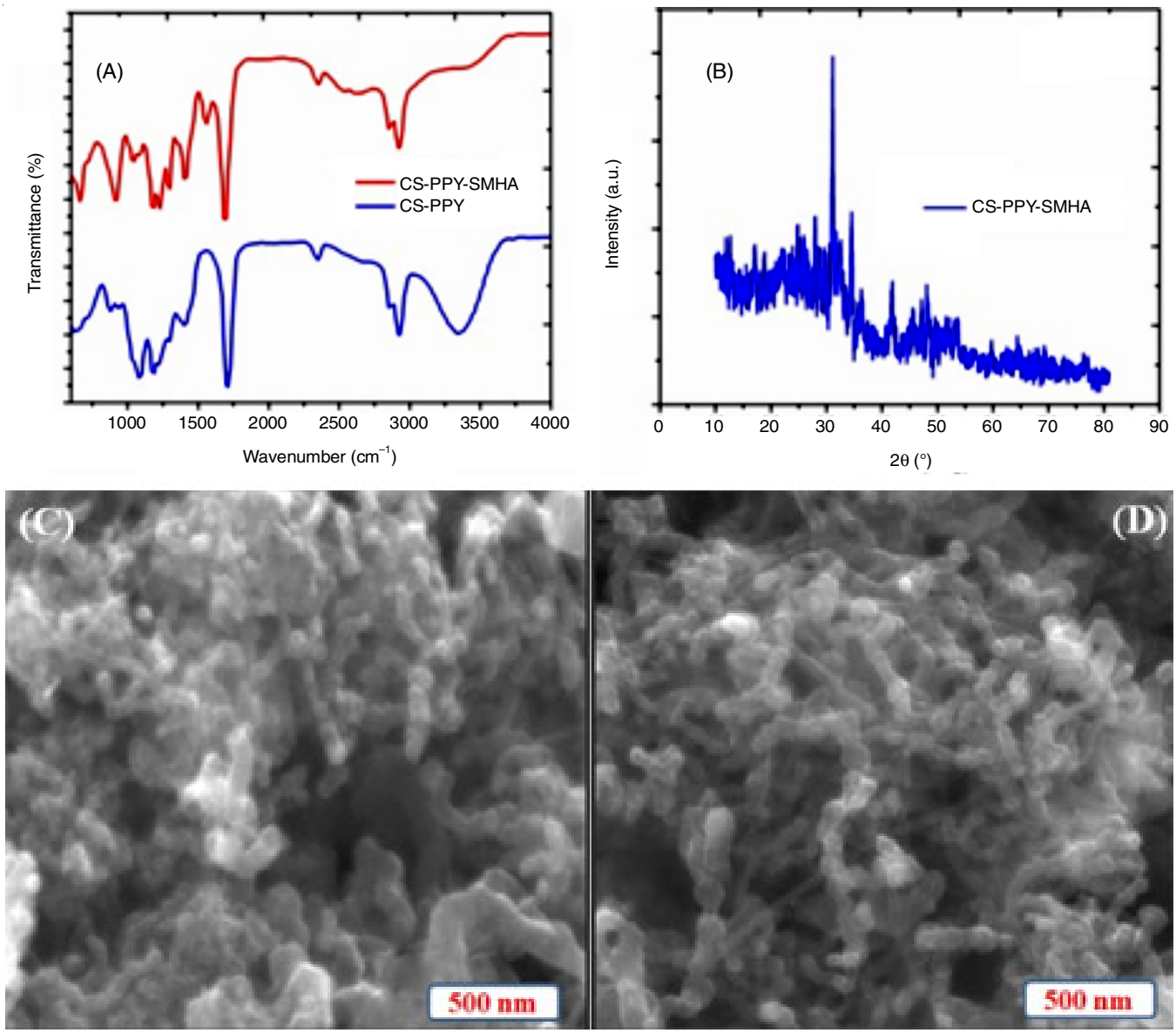


Fig. 2. (a) FTIR spectra (b) X-ray diffraction spectra of biocomposite (c) SEM image of CS-PPY and (d) SEM image of CS-PPY-SMHA biocomposite

FTIR findings was almost similar to an earlier work of Sroka-Bartnicka *et al*. [24].

The X-ray diffraction patterns of CS-PPY-SMHA biocomposite were revealed in Fig. 2b. The presence of the typical crystalline bands at 2θ = 26º, 32º, 42º, 50º, *etc*. for CS-PPY-SMHA biocomposite scaffolds related to (0 0 2) and (2 1 1) SMHA planes confirming the inclusion of SMHA in the biocomposite scaffolds [25].

The porous morphology with interconnected porosity and the pore volume size of CS-PPY and CS-PPY-SMHA are 255 and 192 µm respectively. Both biocomposites revealed (Fig. 2c-d) as micro-size (100-250 µm), which is useful in tissue engineering for substance supplication [26]. This interconnected porosity is vital to the absorption of nutrients and excretions in the physiological system by ligament scaffolds. The compressive strength of load-bearing biocomposite does not affect these small pores. They disburse load more uniformly, however, and serve as a barrier to crack proliferation, which affects the capacity of fatigue. Therefore, it decreases the porosity and thus more fluid barriers and therefore increases the value of the fluid charge [27].

## Mechanical properties

Although scaffolds are supposed to vanish after *in vivo* implantation, the scaffolds need a certain degree of mechanical strength to sustain a certain amount of biological load [28]. Several factors that contribute to the mechanical properties of multi-phase biocomposite scaffolds, including particle size of inorganic constituents, intrinsic physical characteristics of organic constituents, interfacial interfaces between organic and inorganic constituents, organic/inorganic material ratio and cross-linking nature. The mechanical properties of biocomposite scaffolds CS-PPY, SMHA and CS-PPY-SMHA were evaluated (Table-1). Contrasted to the SMHA scaffold, the CS-PPY scaffold

demonstrated lower tensile strength. Adding SMHA nanoparticles to the CS-PPY scaffold matrix, therefore improved its tensile strength. Present findings appear to be consistent with the previous studies [29].

TABLE-1
MECHANICAL PROPERTIES OF THE BIOCOMPOSITE

| Samples | Tensile strength (kPa) | Young's modules (MPa) | Compressive strength (MPa) |
|---|---|---|---|
| Cs-PPY | 710 | 19.13 | 5.2 |
| CS-PPY-SMHA | 1551 | 30.45 | 7.03 |

**Swelling studies:** The results indicate that the addition of SMHA nanoparticles will cause biocomposite scaffold swelling [30]. The introduction of SMHA nanoparticles reduced bio-composite scaffolding matrix swelling leading to the creation of a barrier layer prohibiting water permeability in the biocomposite scaffold (Fig. 3). Some hydrophilic groups of biomolecules were also concerned caused by the interaction between polymer matrix, SMHA and the solution absorption was reduced, which decreases the swelling. Diminishing swelling behaviour can also affect the tensile strength of biocomposite scaffolds.

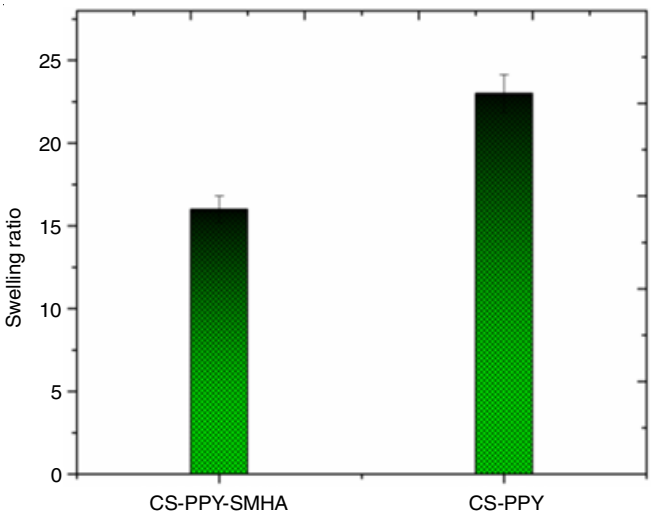


Fig 3. Swelling behaviour of biocomposite in PBS

**Biodegradation:** The biodegradation activity of biomaterials plays a significant role in the development phase of new tissue in metabolic conditions [31]. Fig. 4A demonstrates the CS-PPY and CS-PPY-SMHA biocomposite scaffolds in PBS-containing lysozyme in *ex vivo* biodegradation results. This showed that the percentage of biodegradation was somewhat minimized by the introduction of SMHA nanoparticles. In the CS-PPY-SMHA biocomposite scaffold, the biodegradation was minimized relative to the CS-PPY matrix by the introduction of SMHA nanoparticles. That is because the sensitivity of buffer media is reduced in polysaccharides.

**Alkaline phosphatase activity (ALP) activity:** Fig. 4B shows an increased activity *ex vivo* ALP of osteoblasts grown with CS-PPY and CS-PPY-SMHA biocomposite scaffolds over time. No substantial difference in ALP activity was found on day 1, though, higher ALP activity was observed for CS-PPY-SMHA biocomposite scaffold after incubation for 7 days contrasted to CS-PPY due to its comparatively porous surface denoting first osteogenic differentiation check-point. The CS-PPY-SMHA biocomposite scaffold should, therefore, provide an important cytocompatible substrate that encourages osteoblast cell differentiation [32].

**Antimicrobial properties:** The agar plates with an inhibition zone (ZOI) against checked microbes are shown in Fig. 5A, which summarizes the width of ZOI around the specimens. All the specimens had a ZOI greater than 3 mm, which indicate that antibacterial activity was superior as per standard SNV 195920-199234 [14]. The presence of the outer, multi-layered membrane consisting of the lipid and polysaccharides O-antigen, outside and an inner core formed by covalent bonds that are normally impermeable and prevent the use of antibiotics is one reason for this poor antibacterial action against *S. aureus*. *E. coli*, therefore, has several layered cell walls made up of teichoic acids, murein and wall-associated associated proteins which degrade rapidly in the presence of OH- group SMHA. The mechanism suggested is consistent with zinc ions′ ability to develop close relations with working protein groups which

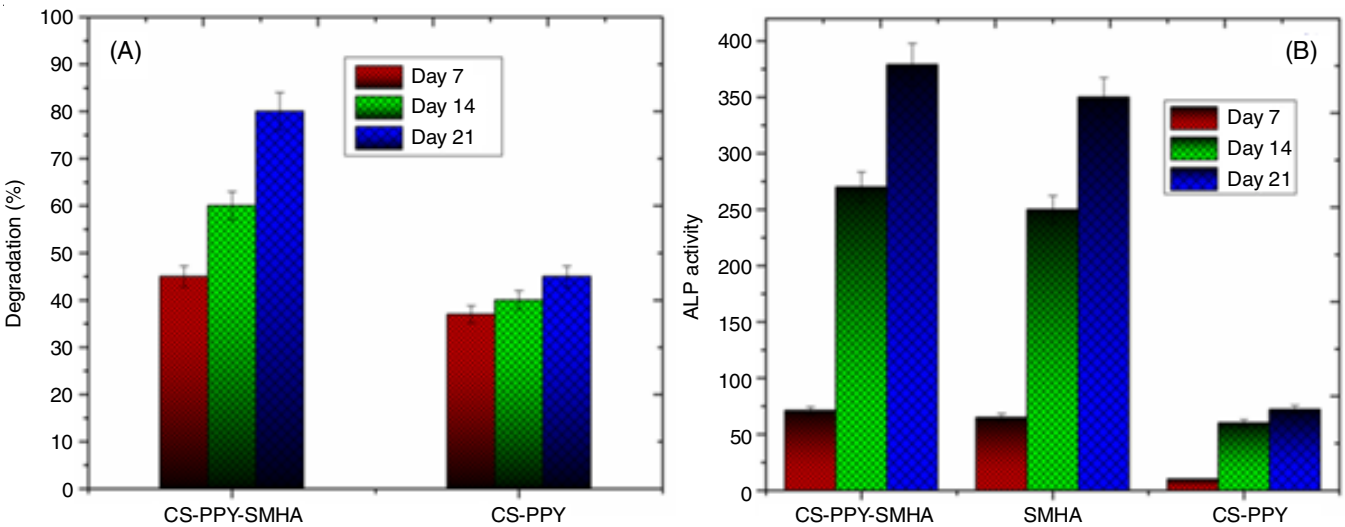


Fig. 4. (a) Biodegradation behaviour of biocomposite in PBS and (b) Alkaline phosphatase activity of biocomposite

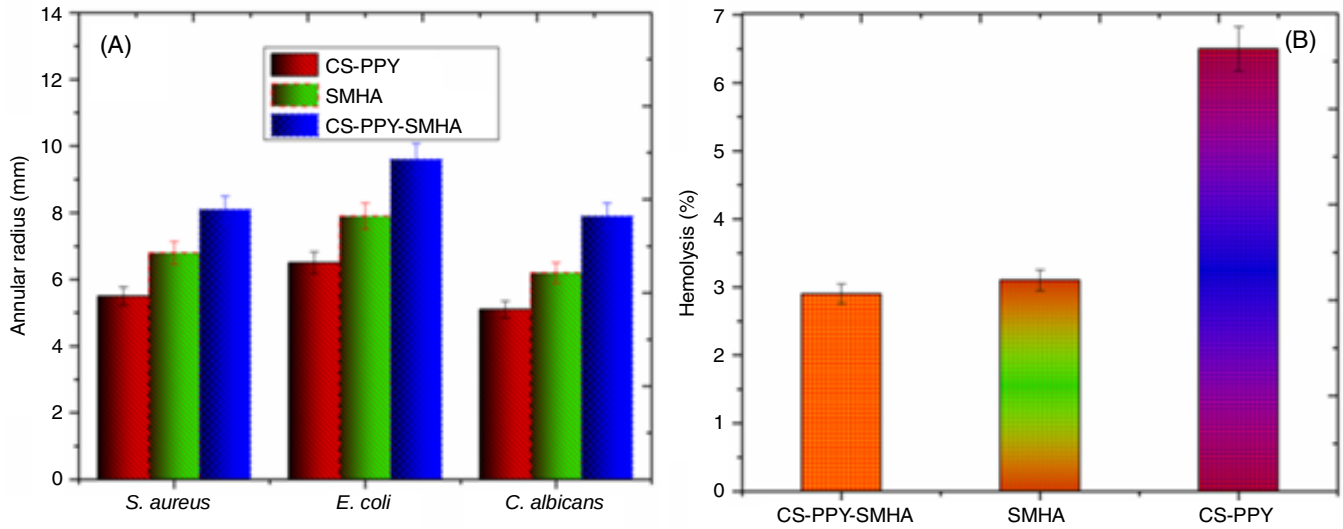


Fig. 5. (a) Antibacterial activity and (b) hemocompatibility of prepared samples

are present in the bacterial cell membranes (severe membrane damage, as metal ions affect the membrane).

**Hemolysis assay:** All the prepared biocomposite specimens were read for blood-compatibility as shown in Fig. 5b. The estimation of the percentage of hemolysis for all the samples was under 5% hemolysis demonstrated that the samples were profoundly blood-compatible. The percentage of hemolysis esteem was seen as diminished with increment in the joining of co-adapted SMHA into the CS-PPY, while the unadulterated biocomposite demonstrated more prominent percentage hemolysis of 2.91% which lies under 5% hemolysis. Thus, all the samples arranged demonstrated the percentage of hemolysis under 5%, so they all can be utilized for biomedical application [33].

**Cytotoxicity assay:** MTT assay was used to assess the *in vitro* biocompatibility of the biocomposite against osteoblast cell lines [34]. The mammalian cell viability of the treated samples DMEM (control), CS-PPY, SMHA and CS-PPY-SMHA (Fig. 6). The potential cytotocompatibility of CS-PPY, SMHA and CS-PPY-SMHA biocomposite was estimated and compared with the DMEM. The DMEM shows the highest cell proliferation (100%) and SMHA with CS-PPY-SMHA ($90 \pm 0.52\%$ and $98 \pm 0.20\%$) demonstrated a greater cell viability than CS-PPY ($84 \pm 0.25\%$). It may be attributed to the discharge of calcium, strontium, zinc and phosphate bioactive ions from SMHA that anchors CS-PPY for cell migration and growth. According to ISO criteria for the assessment of bioactivity, biocomposite displayed no toxicity to osteoblast cells, as its relative feasibility was more than 70%.

**Live/dead assay:** Live/death assays were routinely performed to determine the proportion of living cells and dead cells (Fig. 7). As shown, biocomposite scaffolds have in no way inhibited cell proliferation. Compared to the CS-PPY biocomposite scaffolds, the CS-PPY-SMHA biocomposite scaffolds display bright green fluorescence, with no dead cells present. These findings suggested that prepared CS-PPY-SMHA biocomposite scaffold did not exhibit any apparent cytotoxicity to osteoblast cells in 3rd day incubation and are prospective

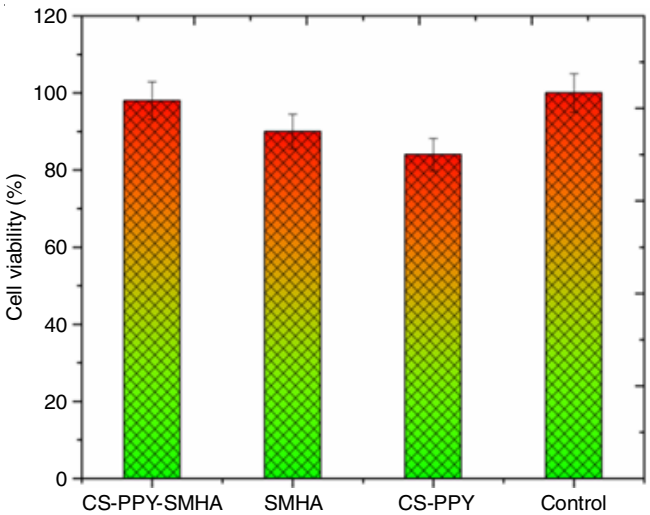


Fig. 6. Osteoblast cell viability on biocomposite towards control (DMEM), CS-PPY, SMHA, and CS-PPY-SMHA biocomposite samples after 3rd day culture

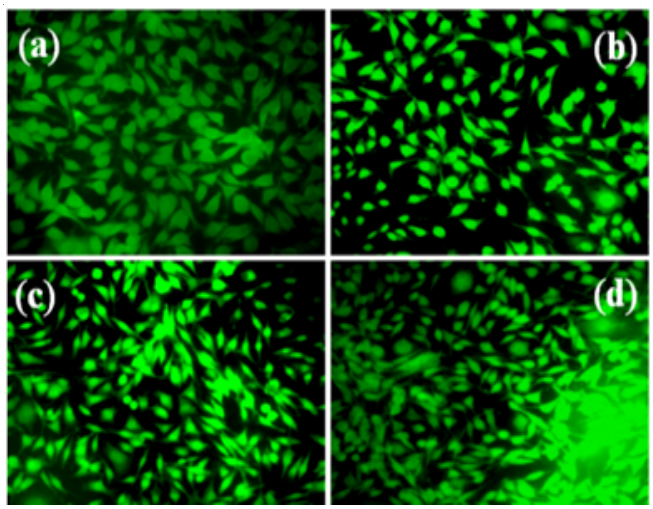


Fig. 7. Morphological examinations of the microscopic images of osteoblast cells cultured for 3rd culture on (a) control (b) CS-PPY (c) SMHA and (d) CS-PPY-SMHA

biomaterials with superior antimicrobial activity without substantial biocompatibility to bone cells.

## Conclusion

In this work, chitosan-polypyrrole composite strengthened by strontium-magnesium substituted hydroxyapatite (SMHA) nanorod was successfully produced with prospective use as regeneration of alveolar bone. The SMHA nanoparticles formed has a single-dimensional rod-like shape with an average diameter of 50 ± 16 nm and a length of 230-650 nm. The porosity in the biocomposite with intertwined permeability was identified both on the surface and in the transversal portion. This may be necessary for the absorption of materials and metabolic functions, as well as for the maintenance of fluid load in diarthrodial bones. The swelling intensity may be decreased as a feature of SMHA nanoparticles suggested that the additional bonding is affected by the strength. Significant changes in the mechanical values were observed when a SMHA nanoparticle was integrated into the CS-PPY matrices. The microbial retentive of biocomposite against checked pathogens has been adequate and integration of SMHA into CS-PPY improves cytocompatibility demonstrating more than 90% vitro cytotoxicity responses of osteoblast cell after 3rd day of culture. Thus, agreed with the aforementioned findings, the ideal biomaterial for regenerative medicine bone repair is CS-PPY/SMHA biocomposite.

## CONFLICT OF INTEREST

The authors declare that there is no conflict of interests regarding the publication of this article.

## REFERENCES


1. A.D. Kolb and K.M. Bussard, *Cancers*, **11**, 1020 (2019); https://doi.org/10.3390/cancers11071020
2. A.M. Ferreira, P. Gentile, V. Chiono and G. Ciardelli, *Acta Biomater.*, **8**, 3191 (2012); https://doi.org/10.1016/j.actbio.2012.06.014
3. A. Jaggessar, H. Shahali, A. Mathew and P.K.D.V. Yarlagadda, *J. Nanobiotechnol.*, **15**, 64 (2017); https://doi.org/10.1186/s12951-017-0306-1
4. M. Šupová, *Ceram. Int.*, **41**, 9203 (2015); https://doi.org/10.1016/j.ceramint.2015.03.316
5. Y. Xu, L. An, L. Chen, H. Xu, D. Zeng and G. Wang, *Adv. Powder Technol.*, **29**, 1042 (2018); https://doi.org/10.1016/j.apt.2018.01.008
6. B. Huang, Y. Yuan, T. Li, S. Ding, W. Zhang, Y. Gu and C. Liu, *Sci. Rep.*, **6**, 24323 (2016); https://doi.org/10.1038/srep24323
7. Z.B. Huang, G.F. Yin, X.M. Liao and J.W. Gu, *Front. Mater. Sci.*, **8**, 39 (2014); https://doi.org/10.1007/s11706-014-0238-8
8. M. Mu, X. Li, A. Tong and G. Guo, *Expert Opin. Drug Deliv.*, **16**, 239 (2019); https://doi.org/10.1080/17425247.2019.1580691
9. M. Zhai, Y. Xu, B. Zhou and W. Jing, *J. Photochem. Photobiol. B*, **180**, 253 (2018); https://doi.org/10.1016/j.jphotobiol.2018.02.018
10. M.H. Fathi and A. Hanifi, *Mater. Lett.*, **61**, 3978 (2007); https://doi.org/10.1016/j.matlet.2007.01.028
11. M. Mehrabanian and M. Nasr-Esfahani, *Int. J. Nanomedicine*, **6**, 1651 (2011); https://doi.org/10.2147/IJN.S21203
12. M.F. Abou Taleb, A. Alkahtani and S.K. Mohamed, *Polym. Bull.*, **72**, 725 (2015); https://doi.org/10.1007/s00289-015-1301-z
13. J. Venkatesan, R. Pallela, I. Bhatnagar and S.-K. Kim, *Int. J. Biol. Macromol.*, **51**, 1033 (2012); https://doi.org/10.1016/j.ijbiomac.2012.08.020
14. Y.S. Wei, K.S. Chen and L.T. Wu, *J. Inorg. Biochem.*, **164**, 17 (2016); https://doi.org/10.1016/j.jinorgbio.2016.08.007
15. R. Jolly, A.A. Khan, S.S. Ahmed, S. Alam, S. Kazmi, M. Owais, M.A. Farooqi and M. Shakir, *Mater. Sci. Eng. C*, **109**, 110554 (2020); https://doi.org/10.1016/j.msec.2019.110554
16. J. Zhang, G. Liu, Q. Wu, J. Zuo, Y. Qin and J. Wang, *J. Bionics Eng.*, **9**, 243 (2012); https://doi.org/10.1016/S1672-6529(11)60117-0
17. V. Trakoolwannachai, P. Kheolamai and S. Ummartyotin, *Int. J. Biol. Macromol.*, **134**, 557 (2019); https://doi.org/10.1016/j.ijbiomac.2019.05.004
18. A.G. Santos, G.O. da Rocha and J.B. de Andrade, *Sci. Rep.*, **9**, 1 (2019); https://doi.org/10.1038/s41598-018-37186-2
19. S. Suresh and A. Dakshnamoorthy, *Int. J. Phys. Sci.*, **8**, 1639 (2013); https://doi.org/10.5897/IJPS2013.3990
20. M.A. Nazeer, E. Yilgör and I. Yilgör, *Carbohydr. Polym.*, **175**, 38 (2017); https://doi.org/10.1016/j.carbpol.2017.07.054
21. S. Utara and J. Klinkaewnarong, *Ceram. Int.*, **41**, 14860 (2015); https://doi.org/10.1016/j.ceramint.2015.08.018
22. S. Yalçinkaya, C. Demetgül, M. Timur and N. Çolak, *Carbohydr. Polym.*, **79**, 908 (2010); https://doi.org/10.1016/j.carbpol.2009.10.022
23. L. Pighinelli and M. Kucharska, *Carbohydr. Polym.*, **93**, 256 (2013); https://doi.org/10.1016/j.carbpol.2012.06.004
24. A. Sroka-Bartnicka, L. Borkowski, G. Ginalska, A. Slósarczyk and S.G. Kazarian, *Spectrochim. Acta A Mol. Biomol. Spectrosc.*, **171**, 155 (2017); https://doi.org/10.1016/j.saa.2016.07.051
25. J. Han, Z. Zhou, R. Yin, D. Yang and J. Nie, *Int. J. Biol. Macromol.*, **46**, 199 (2010); https://doi.org/10.1016/j.ijbiomac.2009.11.004
26. J.Y. Shin, S.J. Jeong and W.K. Lee, *J. Ind. Eng. Chem.*, **80**, 862 (2019); https://doi.org/10.1016/j.jiec.2019.07.042
27. L. Du, W. Li, Z. Jiang, L. Wang, D. Kong, B. Xu and M. Zhu, *Mater. Lett.*, **236**, 1 (2019); https://doi.org/10.1016/j.matlet.2018.10.040
28. L. Zhang, B. Song, L. Yang and Y. Shi, *Acta Biomater.*, **112**, 298 (2020); https://doi.org/10.1016/j.actbio.2020.05.038
29. M. Li, Y. Guo, Y. Wei, A.G. MacDiarmid and P.I. Lelkes, *Biomaterials*, **27**, 2705 (2006); https://doi.org/10.1016/j.biomaterials.2005.11.037
30. A. Hasan, G. Waibhaw, V. Saxena and L.M. Pandey, *Int. J. Biol. Macromol.*, **111**, 923 (2018); https://doi.org/10.1016/j.ijbiomac.2018.01.089
31. M. Ezati, H. Safavipour, B. Houshmand and S. Faghihi, *Prog. Biomater.*, **7**, 225 (2018); https://doi.org/10.1007/s40204-018-0098-x
32. F. Shi, J. Li, J. Sun, H. Huang, X. Su and Z. Wang, *Talanta*, **207**, 120341 (2020); https://doi.org/10.1016/j.talanta.2019.120341
33. S. Braune, A. Lendlein and F. Jung, Hemocompatibility of Biomaterials for Clinical Applications: Blood-Biomaterials Interactions,edn 1, Chap.: Part 1-3, pp. 51-76 (2018).
34. L. Chen, J.M. Mccrate, J.C.M. Lee and H. Li, *Nanotechnology*, **22**, 105708 (2011); https://doi.org/10.1088/0957-4484/22/10/105708